Am J Cardiovasc Dis 2025;15(4):223-234
www.AJCD.us /ISSN:2160-200X/AJCD0165416

Original Article

Circulating extracellular RNAs, myocardial remodeling, and elevated BMI in patients with acute coronary syndrome

Katherine A Tak[1*], Darleen Lessard[2], Peng Zhou[2], Chan Zhou[2], Catarina I Kiefe[2], Matthew Parker[1], Gerard P Aurigemma[1], David D McManus[1,2], Khanh-Van Tran[1]

[1]*Department of Medicine, University of Massachusetts Chan Medical School, Worcester, MA, USA;* [2]*Department of Quantitative Health Sciences, University of Massachusetts Chan Medical School, Worcester, MA, USA*

Received April 17, 2025; Accepted July 8, 2025; Epub August 15, 2025; Published August 30, 2025

Abstract: Objective: Given the elevated mortality in individuals with acute coronary syndrome and increased adiposity, delineating the molecular mechanisms underlying obesity-associated adverse cardiac remodeling is critical for the identification of novel pathophysiological biomarkers and potential therapeutic targets. Circulating extracellular RNAs (ex-RNAs) regulate important biological processes and can serve as biomarkers of disease. This study aims to discover circulating extracellular RNAs (ex-RNAs) that serve as biomarkers of obesity-associated adverse cardiac remodeling in ACS survivors. Methods: We analyzed extracellular RNA (ex-RNA) profiles in 296 survivors of acute coronary syndrome enrolled in the Transitions, Risks, and Actions in Coronary Events - Center for Outcomes Research and Education (TRACE-CORE) cohort. A total of 317 ex-RNAs were quantified, selected a priori based on prior findings from a large population-based study. We employed a two-step, mechanism-driven approach to identify ex-RNAs associated with echocardiographic phenotypes, including left atrial (LA) dimension, LA volume index, left ventricular (LV) ejection fraction, LV mass, and LV end-diastolic volume, then tested the relations of these ex-RNAs with obesity. We performed further bioinformatics analysis of the gene ontology categories and molecular pathways associated with predicted miRNA targets. Results: We identified 45 ex-RNAs associated with at least one echocardiographic phenotype, of which miR-1185-1-3p, miR-550a-3p, and miR-885-5p were also associated with prevalent obesity. Bioinformatic analysis of their predicted gene targets (n=1,930) revealed enrichment in key pathways related to inflammation, fibrosis, and cellular toxicity, including Wnt/β-catenin signaling, TGF-β signaling, and hypoxia-inducible factor (HIF) signaling. Targets such as DICER1, VEGF, and EPO were implicated. Gene ontology analysis further highlighted associations with angiogenesis, FGF signaling, and interleukin pathways. Conclusions: Among ACS survivors, we observed that miR-1185-1-3p, miR-550a-3p, and miR-885-5p were associated with both echocardiographic markers of adverse cardiac remodeling and elevated BMI. Relevance for patients: miR-1185-1-3p, miR-550a-3p, and miR-885-5p were associated with echocardiographic phenotypes and obesity and are potential biomarkers for adverse cardiac remodeling in obesity.

Keywords: Extracellular RNA, microRNA, body mass index, acute coronary syndrome

Introduction

Acute coronary syndromes (ACS) remain a leading cause of cardiovascular morbidity and mortality worldwide, and identifying molecular and structural markers of adverse cardiac remodeling in ACS patients is critical for improving clinical outcomes [1-3]. Among ACS survivors, several patient characteristics, including elevated body mass index (BMI), are known to influence cardiac remodeling and recovery trajectories [4, 5]. Interestingly, while obesity is generally associated with increased cardiovascular risk, in the setting of established cardiovascular disease (CVD) and ACS, an *obesity paradox* has been observed, whereby overweight and obese patients may exhibit more favorable short and long-term outcomes compared to normal weight individuals [6]. Nonetheless, obesity contributes to maladaptive cardiac remodeling, which is a key determinant of heart failure risk in this population. The molecular mechanisms throu-

https://doi.org/10.62347/HMVT2954

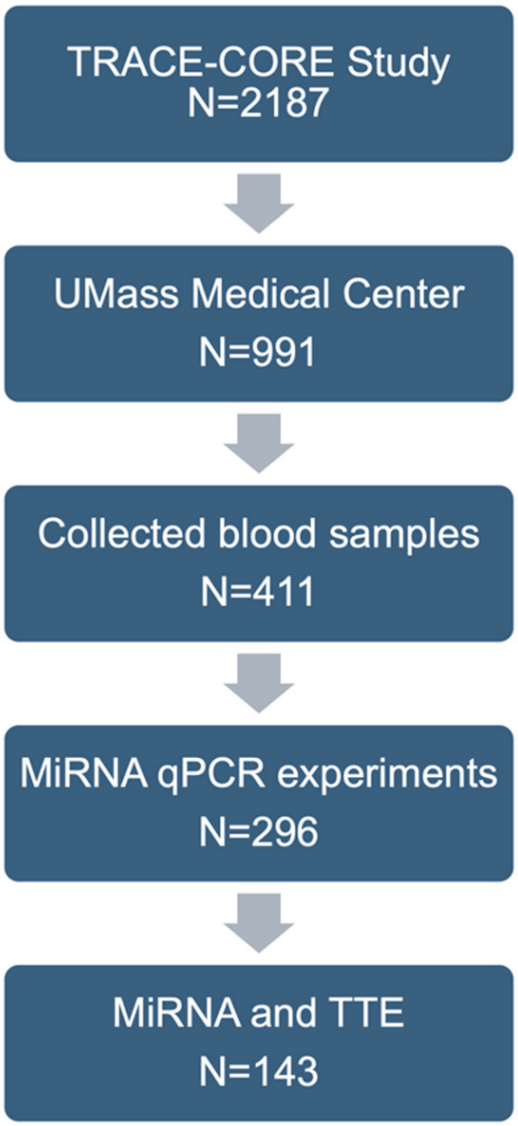

Figure 1. Enrollment, screening, and transcriptomic profiling and echocardiographic measurements of TRACE-CORE Cohort.

gh which increased adiposity influence cardiac remodeling in ACS patients remain poorly understood.

Transthoracic echocardiography (TTE) is a standardized, noninvasive technique which is commonly used to assess cardiac function and for prognostication of adverse cardiac remodeling [7]. Echocardiographic parameters such as enlarged cardiac chamber size, lower left ventricular ejection fraction (LVEF), and higher left ventricular mass (LV mass) have been associated with the incidence of obesity, and represent adverse remodeling in this disease process [8, 9]. The high utility of echocardiography in the evaluation and prognostication of adverse cardiac remodeling is due to its ability to describe structural processes involved in pathological cardiac remodeling. Circulating extracellular RNAs (ex-RNAs), including microRNAs (miRNAs), have also emerged as promising biomarkers of cardiovascular stress and remodeling. Ex-RNAs are endogenous small noncoding RNAs that circulate in the plasma with remarkable stability and variable expression [10]. While miRNAs are known to regulate intracellular signaling processes, circulating miRNAs have also been shown to serve as biomarkers in several disease processes [11, 12].

To better understand the molecular signaling pathways implicated in patients with elevated BMI (BMI >25, including both overweight and obese individuals), we examined the ex-RNAs known to be involved in both cardiac remodeling and elevated BMI in a patient population hospitalized acutely for ACS. We employed a two-step analysis model that connected miRNA to both echocardiographic phenotypes associated with cardiac remodeling and elevated BMI in ACS survivors from the Transitions, Risks, and Action in Coronary Events Center for Outcomes Research and Education (TRACE-CORE) cohort [13]. Our objective was to identify candidate ex-RNAs which were highly expressed in hospitalized ACS patients with elevated BMI, aiming to uncover the molecular pathways linking elevated BMI to adverse cardiac remodeling in this high-risk population.

Materials and methods

Study population

An in-depth description of the design, recruitment, interview, and medical record abstraction procedures used in the TRACE-CORE study have previously been reported [13, 14]. Briefly, TRACE-CORE is a 6-site prospective cohort study comprised of 2,187 patients discharged after an ACS hospitalization from April 2011 to May 2013 (**Figure 1**). Inclusion required ACS symptoms plus ≥1 of the following: serial ECG changes, elevated cardiac biomarkers, >70% coronary stenosis on catheterization, or urgent/emergent PCI or CABG with ischemic symptoms within 72 hours. Exclusion criteria were as follows: ACS due to aortic dissection or demand

ischemia, hospice/palliative care, dementia, perioperative ACS, trauma, pregnancy, incarceration, transfer after >24-hour hospitalization elsewhere, or elective PCI/CABG without preceding symptoms. ACS diagnoses were confirmed by discharge review and cardiologist adjudication. Two academic teaching hospitals and one large community hospital were included in Central Massachusetts. The other sites were two hospitals affiliated with a managed care organization in Atlanta, GA, and an academic medical center in central Georgia. At the Central Massachusetts sites, 411 blood samples were collected and processed as described previously, and plasma was stored in -80°C [10, 15]. 296 of the collected plasma samples were of sufficient quality for RNA extraction and qPCR studies. All participants provided written informed consent. This study was approved by the institutional review boards at each participating recruitment site.

BMI classification

Study participants were stratified into three groups by BMI, using the Centers for Disease Control (CDC) BMI classification. A BMI between 18.5 to less than 25 kg/m^2 was classified as healthy weight, between 25 and 30 kg/m^2 was classified as overweight, and obesity was classified as a BMI of ≥35 kg/m^2 [16].

Ex-RNA selection and profiling

Venous blood samples were collected during the index hospitalization of 296 participants enrolled in the TRACE-CORE cohort for transcriptomic profiling. Protocols for blood sample processing, plasma storage, and RNA isolation have been previously described [15]. The quantification of ex-RNAs, including miRNAs and small nucleolar RNAs (snoRNAs), was conducted according to a previously reported methodology [10]. The selection of ex-RNAs for profiling was performed *a priori*, based on prior findings from the Framingham Heart Study [10]. Plasma ex-RNA profiling was conducted at the High-Throughput Gene Expression and Biomarker Core Laboratory at the University of Massachusetts Chan Medical School. Quantification was expressed using quantification cycle (Cq) values, with a higher Cq indicating lower ex-RNA abundance. This approach identified 331 miRNAs and 43 snoRNAs in total. Detailed profiling results are provided in Supplementary Table 1.

Echocardiographic measurements

Two-dimensional (2D) TTEs were obtained during the index hospitalization. Quantitative assessments were performed in accordance with the American Society of Echocardiography (ASE) guidelines [17]. Measurements included LVEF, left atrial (LA) volume, LA volume index (LAVI), LV mass, and LV end-diastolic volume (LVEDV). LVEF and volume measurements were derived using the biplane method of disks (modified Simpson's) from apical 2- and 4-chamber views. LV mass was calculated using the formula: LV mass =0.8 (1.04[LVID+PWTd+SWTd]3-[LVID]3)+0.6 g, where LVIDd is the LV internal diameter at end-diastole, and PWTd and SWTd represent the posterior wall thickness and septal wall thickness at end-diastole, respectively [18].

Statistical analysis

There are 143 cases with both ex-RNA and echocardiographic data in our TRACE-CORE cohort (**Figure 1**). We used this modified group to identify the ex-RNAs significantly related to at least one echocardiographic parameter. Using this significant list of ex-RNAs, we queried for a relationship with elevated BMI on the full 296 cases with ex-RNA data.

A two-step analysis model was used for this analysis. In Step 1, we used an ordinary least-squares linear regression to quantify the associations between ex-RNA levels and at least one of the echocardiographic phenotypes listed above in section 2.4 in all participants (Supplementary Table 2). We employed Bonferroni correction to establish a more restrictive threshold for defining statistical significance to account for multiple testing. We then used a 5% false discovery rate via the Benjamini-Hochberg false discovery rate approach to screen for associations between ex-RNAs and one or more echocardiographic phenotypes. The α for achieving significance was set at 0.05/340=0.000147 a priori. Of note, Cq represents a log measure of concentration, with an exponentiation factor of 2.

In Step 2, we examined the associations of all ex-RNAs with BMI. Those with statistically sig-

Table 1. Characteristics of TRACE-CORE participants included in the analytic sample

Variable	Healthy Weight BMI 18.5-24.9 (n=53)	Overweight BMI 25-29.9 (n=125)	Obese BMI >30 (n=114)	*p* value*
Age (years)	66.0±11.5	64.5±12.8	60.9±10.1	**0.01**
Female	28.3 (15)	29.6 (37)	36.8 (42)	0.21
Caucasian Race	98.1 (53)	97.6 (122)	95.6 (109)	0.19
Height (inches)	68.2±4.2	68.5±9.5	70.2±18.9	0.55
Weight (lbs)	151.3±27.8	174.2±34.0	220.2±47.7	**<0.001**
Body Mass Index (kg/m^2)	23.1±1.3	27.4±1.5	34.7±4.6	**<0.001**
Risk Factors				
Hyperlipidemia	62.3 (33)	64.8 (81)	75.4 (86)	0.052
Myocardial Infarction	24.5 (13)	27.2 (34)	36.0 (41)	0.09
Anginal Pectoris/CHD	26.4 (14)	24.0 (30)	33.3 (38)	0.22
Type 2 Diabetes Mellitus	11.3 (6)	24.8 (31)	42.1 (48)	**<0.001**
Stroke/TIA	1.9 (1)	3.2 (4)	0.9 (1)	0.48
Atrial Fibrillation	15.1 (8)	7.2 (9)	9.7 (11)	0.44
Hypertension	67.9 (36)	66.4 (83)	75.4 (86)	0.21
Seattle Angina Questionnaire				
Physical Limitation	82.2±22.6	84.9±21.9	78.3±23.6	0.11
Angina Stability	38.6±23.4	45.8±26.2	42.7±31.0	0.32
Angina Frequency	76.2±25.4	78.9±19.7	69.3±25.8	**0.01**
Treatment Satisfaction	92.7±14.1	93.6±11.2	94.6±9.9	0.58
Quality of Life	64.4±29.5	69.1±24.3	58.2±25.7	**0.01**
Admission Medications				
Aspirin	49.1 (26)	44.8 (56)	53.5 (61)	0.41
Beta Blocker	37.7 (20)	39.2 (49)	50.9 (58)	0.06
ACEI or ARB	45.3 (24)	30.4 (38)	47.4 (54)	0.34
Statin	54.7 (29)	53.6 (67)	67.5 (77)	0.052
Plavix	9.4 (5)	10.4 (6)	20.2 (3)	**0.03**
Coumadin	9.4 (5)	4.8 (13)	7 (23)	0.75
Physical Activity				
No Physical Acitivity	58.8 (30)	59.4 (73)	62.3 (71)	
<150 min/wk	15.7 (8)	15.5 (19)	15.8 (18)	0.56
>150 min/wk	25.5 (13)	25.2 (31)	21.9 (25)	
Acute Coronary Syndrome Category				
ST-elevation myocardial infarction	30.2 (16)	22.4 (28)	27.2 (31)	0.9
Physiological Factors				
Heart rate (beats per minute)	81.7±20.00	75.5±21.3	81.5±22.4	0.06
Systolic blood pressure (mmHg)	136.9±28.2	140.3±24.1	140.2±23.7	0.68
Diastolic blood pressure (mmHg)	77.1±20.4	78.7±15.3	79.6±16.0	0.68
Respiratory rate (breaths per minute)	18.9±5.0	17.8±3.9	18.6±4.0	0.17
Electrocardiogram				
QRS duration	159.8±40.3	168.2±28.2	165.8±25.8	0.28
PR interval	97.7±23.6	96.0±20.0	99.1±22.7	0.56
Lab Values				
Troponin peak	25.5±39.3	22.2±31.6	25.3±38.8	0.78
Total cholesterol	174.6±39.1	174.2±50.9	167.5±44.7	0.4
Creatinine	1.2±0.53	1.2±0.33	1.3±0.67	0.56
Hemoglobin	10.9±2.2	11.8±2.2	11.7±2.3	0.051
Sodium	136.1±2.9	135.4±3.7	135.8±3.2	0.49

Echocardiographic Phenotype‡				
LVEF	52.62±14.59	52.84±12.11	52.79±12.73	0.99
LA volume	46.57±17.57	47.30±22.28	48.20±19.54	0.96
LAVI	25.28±8.18	23.94±10.15	22.87±8.57	0.63
LV mass	167.99±51.12	184.51±62.31	196.56±59.42	0.16
LVEDV	81.43±38.65	87.71±40.04	91.37±46.74	0.67

Data represented as mean ± standard deviation or percentage (count). Legend: TRACE-CORE: Transitions, Risks, and Actions in Coronary Events Center for Outcomes Research and Education; CHD: coronary heart disease; TIA: transient ischemic attack; ACEi: angiotensin-converting enzyme inhibitors; ARB: angiotensin II receptor blockers. LVEF = left ventricular (LV) ejection fraction, LAVI = LA volume index, LVEDV = left ventricular (LV) end-diastolic volume. *P<0.05 are in bold. ‡ Echocardiographic phenotypes were analyzed in a subset of patients (n=133) in whom TTE was available.

Table 2. Associations between BMI and miRNAs

MiRNA ID	b-Coefficient	95% Confidence Intervals		*p*-Value
hsa_miR_103a_3p	1.09849	0.19268	2.0043	0.0186
hsa_miR_1185_1_3p	**-0.75356**	**-1.22703**	**-0.28009**	**0.00465**
hsa_miR_1226_3p	0.68544	0.14816	1.22273	0.013279
hsa_miR_182_5p	-0.72922	-1.32758	-0.13086	0.017947
hsa_miR_19a_3p	-0.54137	-1.02493	-0.0578	0.028383
hsa_miR_203a	0.87709	0.10299	1.65119	0.026852
hsa_miR_23a_3p	-0.39561	-0.79023	-0.00099	0.049432
hsa_miR_31_3p	-0.83147	-1.56467	-0.09827	0.034562
hsa_miR_335_3p	-0.7535	-1.30766	-0.19935	0.009169
hsa_miR_550a_3p	**-1.09491**	**-1.56429**	**-0.62553**	**0.001851**
hsa_miR_885_5p	**-0.37142**	**-0.73192**	**-0.01092**	**0.043621**

Bolded are miRs also related to echocardiographic phenotypes.

nificant associations are shown in **Table 2**. Notably, the number of participants in each step differed as we did not have echocardiographic data available for all participants with plasma ex-RNA data. We examined the associations between miRNAs identified from Step 1 and BMI using a logistic regression model. In this step, we used continuous Cq values for comparison with BMI (**Table 2**).

The targets of the three most highly differentially expressed miRNAs were then acquired using miRDB, an online database that captures miRNA and gene target interactions [19]. We acknowledge our use of the gene set enrichment analysis software and molecular signature database (geneontology.org) for ontology analysis using the Protein Analysis THrough Evolutionary Relationships (PANTHER) annotated dataset [20]. The work and functional analyses were then generated using Qiagen's Ingenuity Pathway Analysis (IPA) version 24.0.2 [21]. All statistics were performed with SAS software version 9.3 (SAS Institute) with a 2-tailed P< 0.05 as significant.

Results

Patient characteristics

The baseline demographic, clinical, and echocardiographic characteristics of the 292 study participants are outlined in **Table 1**. The mean age of participants in the healthy weight, overweight, and obese groups were 66.0±11.5 (n=53), 64.5± 12.8 (n=125), and 60.9±10.1 (n=114), respectively (P=0.01). The overweight and obese groups had significantly higher prevalent type 2 diabetes mellitus compared to the healthy weight group, at 24.8% and 42.1% respectively vs. 11.3% (P<0.001). Interestingly, we observed no significant differences in LVEF, LA volume, LAVI, LV mass, or LVEDV between the three groups. We did observe a concordant trend of increasing LA volume, LV mass, and LVEDV with increasing BMI, though this was not statistically significant.

Association of ex-RNAs with echocardiographic phenotypes

In total, 374 ex-RNAs (331 miRNAs and 43 snoRNAs) were quantified in the plasma of TRACE-CORE participants and included in our investigation. Of these, 45 ex-RNAs were associated with at least one echocardiographic parameter independent of other clinical variables (Supplementary Table 2). Three miRNAs, miR-190a-3p, miR-596, and miR-885-5p, were

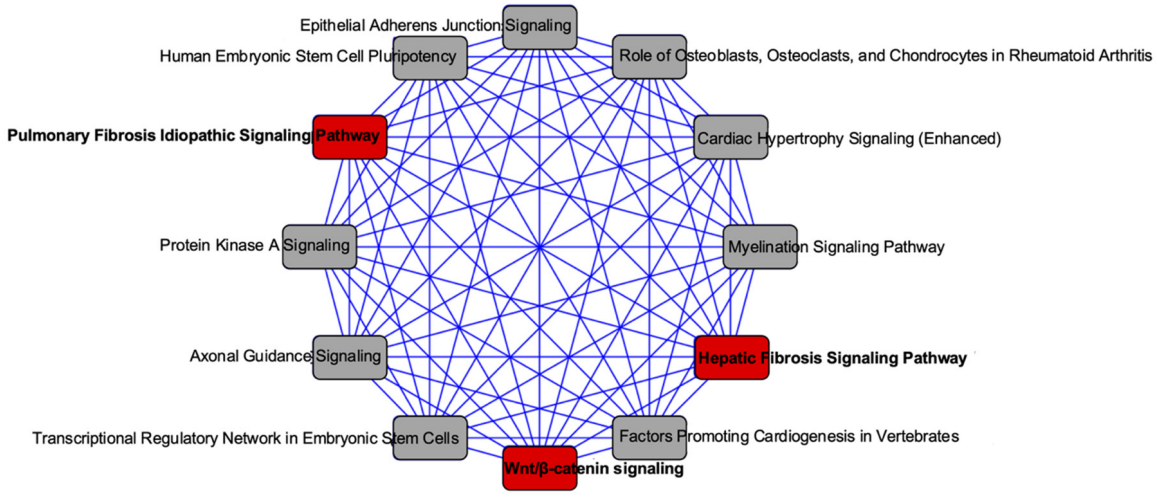

Figure 2. Overlapping canonical pathways analysis of the predicted targets of miR-1185-1-3p, miR-550a-3p, and miR-885-5p as performed by ingenuity pathway analysis (IPA). Nodes represent signaling pathways, and lines are protein targets that are common between nodes. Highlighted in red are pathways previously associated with inflammation, cardiac necrosis, and fibrosis.

associated with three or more echocardiographic parameters (Supplementary Table 2).

Associations of ex-RNAs with BMI

Eleven ex-RNAs were identified to be significantly correlated with increasing BMI, many of which were inversely correlated (**Table 2**). Three of these, miR-1185-1-3p, miR-550a-3p, and miR-885-5p, were also correlated with at least one echocardiographic phenotype.

Gene targets of ex-RNAs associated with elevated BMI

We then used miRDB to investigate the predicted targets of miR-1185-3p, miR-550a-3p, and miR-885-5p. Between the three miRNAs, 1,930 genes were predicted as targets. Recognizing that miRNAs act in concert, we leveraged the combined target list for further analysis [22]. IPA was utilized to identify the molecular networks regulated by these targeted genes, as well as the subset of targeted genes known to be involved in cellular toxicity pathways. Overlapping canonical pathways were mapped out to visualize these shared biological pathways (**Figure 2**). Identified nodes included Wnt/β-catenin signaling, epithelial adherens junction signaling, the pulmonary fibrosis idiopathic signaling pathway, the hepatic fibrosis signaling pathway, and the role of osteoblasts, osteoclasts and chondrocytes in rheumatoid arthritis. Highlighted in **Figure 2** are the pathways implicated in fibrosis, inflammation, and cell death. The toxicity pathways of the predicted targets included cardiac fibrosis, TGF-β signaling, and hypoxia-inducible factor (HIF) signaling (Supplementary Table 3). Notably, DICER1 and EPO were among the targets identified, which are known to be associated with the TGF-β and HIF signaling pathways [23-25]. PANTHER terms enrichment analysis using geneontology.org showed that miRNAs associated with echocardiographic phenotypes and elevated BMI have strong associations with pathways involved in angiogenesis and fibroblast growth factor (FGF) and interleukin (IL) signaling (**Figure 3**; Supplementary Table 4). These findings are supported in the literature, as miR-1185-1-3p has been shown to be overexpressed in weight loss, and levels have been inversely correlated with IL-6 [26]. miR-885-5p has been shown to be upregulated in fetal hepatocytes exposed to maternal obesity in utero [27]. miR-550a-3p and miR-885-5p promote progression of many cancers [28-33].

Discussion

In our investigation of the ex-RNA profiles of 296 hospitalized ACS survivors in the TRACE-CORE cohort, we identified 45 plasma ex-RNAs associated with at least one echocardiographic trait. Three miRNAs, miR-1185-1-3p, miR-550a-3p, and miR-885-5p, were also associat-

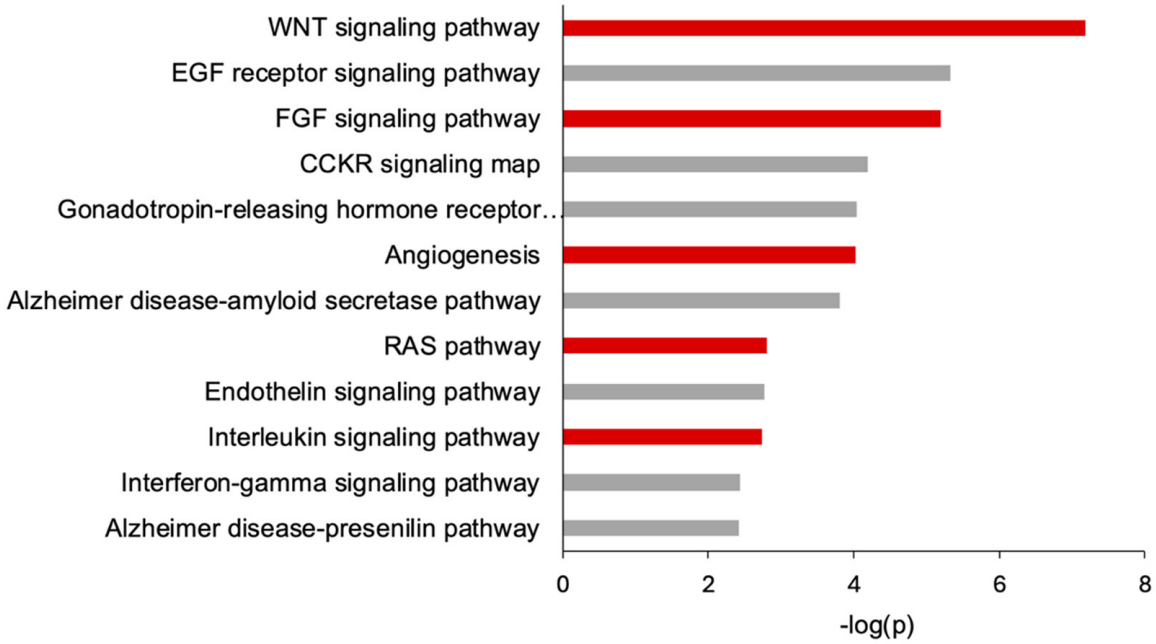

Figure 3. PANTHER term analysis of predicted targets of miR-1185-1-3p, miR-550a-3p, and miR-885-5p as performed by geneontology.org. Labeled in red are terms associated with transforming growth factor-β and hypoxia-inducible factor pathways and in gray are otherwise.

ed with both elevated BMI and cardiac remodeling as determined by echocardiography. While the association of miRNA and elevated BMI has been previously explored, our study uniquely examined the association between ex-RNA and elevated BMI in the acute clinical setting. Although miR-1185-1-3p and miR-885-5p have previously been shown to be associated with elevated BMI [26, 27], this is the first time to our knowledge that miR-550a-3p has been implicated in this disease process.

Echocardiographic phenotypes and cardiac remodeling in relation to elevated BMI

Adverse cardiac remodeling is represented on echocardiography as decreased LVEF with concurrent increased LV mass, LVEDV, LA volume, and LAVI [34-36]. Echocardiographic measures of cardiac remodeling have been correlated with cellular hypertrophy, extracellular collagen deposition, metabolic dysregulation, and myocyte cell death [37]. Although elevated BMI involves several important pathological processes, we focus here on cardiac remodeling, as it is a key factor in the development of cardiac dysfunction. Our analysis shows that increasing LA volume, LV mass, and LVEDV trends with increasing BMI, which aligns with the existing understanding of structural cardiac remodeling in elevated BMI. These observations reinforce the concept that elevated BMI promotes a distinct pattern of structural cardiac remodeling, which may be detectable through circulating molecular biomarkers such as extracellular RNAs (ex-RNAs). Identifying such biomarkers could offer novel insights into the pathophysiological pathways linking obesity to adverse cardiac remodeling and may inform future strategies for risk stratification and early intervention.

Association of ex-RNAs, cardiac remodeling, and elevated BMI

The association of ex-RNAs with cardiac structural remodeling has been previously explored [38]. However, few existing studies have examined quantitative echocardiographic phenotypes in humans in relation to plasma miRNA expression in the context of elevated BMI in patients admitted with ACS. We identified 45 ex-RNAs with statistically significant associations with the pre-specified echocardiographic endophenotypes, three of which were also associated with elevated BMI. Functional analysis of downstream targets supports existing evidence that adverse cardiac remodeling in

elevated BMI is coordinated through several signaling pathways, most notably TGF-β, HIF, and Wnt signaling.

Our analysis suggests that TGF-β plays an integral part in adverse cardiac remodeling in adult ACS survivors with elevated BMI. The TGF-β signalizing pathway partially coordinates the process of tissue fibrosis after cardiac cell death [39-41]. It has also been shown to induce endothelial cells to undergo an endothelial-to-mesenchymal transition, thus contributing to cardiac fibrosis [42]. Serum TGF-β has been associated with BMI and adiposity [43], and has been positively correlated with increasing BMI [44]. Taken together, our data suggest that in ACS survivors, elevated BMI may exacerbate TGF-β-driven cardiac fibrosis and maladaptive remodeling. Circulating ex-RNAs reflecting this fibrotic signature may serve as accessible biomarkers for identifying individuals at heightened risk for progressive cardiac dysfunction after ACS, though further studies are needed to validate these findings.

HIF was also shown in our analysis to be associated with elevated BMI and adverse cardiovascular remodeling. HIF expression in adipocytes has been linked to the development of cardiac hypertrophy via increased levels of proinflammatory cytokines and PPAR-γ [45, 46]. PPAR-γ is known to regulate adipogenesis by decreasing ectopic lipid deposition and increasing insulin sensitivity, which together can increase cardiac hypertrophy [47]. Additionally, HIF-1α facilitates the recruitment of proinflammatory macrophages into both adipose depots and the myocardium, creating an inflammatory environment that promotes fibroblast activation, extracellular matrix deposition, and ultimately cardiac fibrosis and diastolic dysfunction [48].

In addition to TGF-β and HIF pathways, Wnt signaling emerged as another plausible mechanism linking elevated BMI to adverse cardiac remodeling. Wnt signaling regulates adipocyte differentiation and fibroblast activation, both of which are critical to cardiac remodeling [49]. In the setting of elevated BMI, dysregulated Wnt activity can impair adipogenesis, promote inflammatory responses, and facilitate fibrotic transformation of cardiac fibroblasts, thereby exacerbating myocardial stiffness and hypertrophy [50, 51]. Prior studies have shown that Wnt signaling intersects with TGF-β and HIF pathways, further highlighting its integrative role in the pathological remodeling cascade.

PANTHER analysis supports the hypothesis that miR-1185-1-3p, miR-550a-3p, and miR-885-5p play a role in cardiac remodeling through TGF-β, HIF, and Wnt signaling pathways. The top five involved processes are the Alzheimer disease-presenilin pathway, interferon-gamma signaling pathway, interleukin signaling pathway, endothelin signaling pathway, and the RAS pathway. Notably, there is a recurring theme of the PANTHER term enrichment in anti-inflammatory and pro-fibrotic processes, both of which have been shown to be regulated by TGF-β [50, 52, 53]. Together, our data supports the hypothesis that miR-1185-1-3p, miR-550a-3p, and miR-885-5p affect structural cardiac remodeling by influencing adipogenesis, inflammation, and fibrosis, in part through the TGF-β, HIF, and Wnt signaling pathways. Although obesity is often associated with adverse cardiovascular outcomes, this relationship is not universal; adverse cardiac remodeling may be more closely linked to the activation of specific molecular pathways rather than obesity itself.

While we do not find an explicit overlap between our ex-RNAs and those previously identified to be associated with BMI independent of cardiac remodeling, we do find overlap between our miRNAs and those shown to be involved in increasing adiposity. The Rotterdam study examined the association between miRNAs and various measures of elevated BMI and body fat distribution and found 65 miRNAs that were associated with BMI [54]. They identified miR-19a-3p, which we found to be negatively associated with BMI (**Table 2**), to be associated with fat mass index (FMI). This convergence suggests that shared biological pathways may underlie increases in both FMI and BMI, potentially through regulatory effects on adipogenesis, lipid metabolism, or inflammatory signaling.

The lack of more significant overlap between our studies could be due to differences in geographic, demographic, and acuity characteristics between the Rotterdam study and ours. Specifically, the Rotterdam study recruited patients age <55 years only in the Rotterdam district in the Netherlands, whereas our TRACE-CORE cohort included hospitalized patients

with ACS across the United States. These differences highlight the importance of context - including age, geography, and clinical status - when interpreting circulating miRNA signatures, and suggest that while some miRNAs may reflect general adiposity-related processes, others may be more specific to the pathophysiologic setting of acute cardiac events. This highlights the importance of interpreting circulating miRNA signatures within the appropriate clinical and demographic context, and suggests that integrating disease-specific and population level data will be critical for elucidating the mechanistic links between adiposity, inflammation, and cardiovascular remodeling.

Strengths and limitations

Our study has several strengths. We examined the association between ex-RNAs and both echocardiographic traits and BMI in a well-characterized cohort study. TRACE-CORE is a cohort of ACS survivors that allows for interrogation of the plasma ex-RNA expression profiles in the acute clinical setting. While our observations may reflect biomarker changes secondary to ACS rather than elevated BMI, we did not find any significant differences in ex-RNA due to AMI in previous work [55]. Since we employed the similar methods to study ex-RNA in this analysis, the differential expression of ex-RNA is more likely attributable to elevated BMI rather than to ACS status.

Our study has several limitations, including a relatively small sample size that lacks racial and geographic diversity. Although we identified three miRNAs associated with both echocardiographic phenotypes and elevated BMI, the cellular sources of these ex-RNAs and the mechanisms underlying their transport in circulation remain unclear. Further bench experiments are needed to elucidate the molecular mechanisms through which these miRNAs regulate cardiovascular changes associated with elevated BMI.

Conclusions

Through analysis of echocardiographic, clinical, and ex-RNA data from ACS survivors in the TRACE-CORE cohort, we identified miR-1185-1-3p, miR-550a-3p, and miR-885-5p to be candidate circulating biomarkers associated with echocardiographic measures of cardiac remodeling and elevated BMI. These ex-RNAs are predicted to mediate cardiac remodeling in part through the TGF-β, HIF, and Wnt signaling pathways. Further studies in more diverse cohorts, along with mechanistic experiments, are needed to validate and extend our findings.

Acknowledgements

This work is supported by K23HL161432 to KVT and R01HL126911, R01HL137734, R01HL137794, R01HL135219, R01HL136660, U54HL143541, and 1U01HL146382 to DDM from the National Heart, Lung, and Blood Institute.

Disclosure of conflict of interest

DDM has received consultancy fees from Heart Rhythm Society, Fitbit, Flexcon, Pfizer, Avania, NAMSA, and Bristol Myers Squibb. DDM reports receiving research support from Fitbit, Apple, Care Evolution, Boeringher Ingelheim, Pfizer, and Bristol Myers Squibb. KVT has research support for Novartis.

Address correspondence to: Katherine A Tak, Department of Medicine, University of Massachusetts T.H. Chan School of Medicine, Albert Sherman Center, AS7-1057, 368 Plantation St., Worcester, MA 01605, USA. Tel: 508-334-1000; Fax: 774-441-7657; E-mail: katherine.tak@umassmed.edu

References

[1] Di Cesare M, Perel P, Taylor S, Kabudula C, Bixby H, Gaziano TA, McGhie DV, Mwangi J, Pervan B, Narula J, Pineiro D and Pinto FJ. The heart of the world. Glob Heart 2024; 19: 11.

[2] Goodwin NP, Clare RM, Harrington JL, Badjatiya A, Wojdyla DM, Udell JA, Butler J, Januzzi JL Jr, Parikh PB, James S, Alexander JH, Lopes RD, Wallentin L, Ohman EM, Hernandez AF and Jones WS. Morbidity and mortality associated with heart failure in acute coronary syndrome: a pooled analysis of 4 clinical trials. J Card Fail 2023; 29: 1603-1614.

[3] Timmis A, Kazakiewicz D, Townsend N, Huculeci R, Aboyans V and Vardas P. Global epidemiology of acute coronary syndromes. Nat Rev Cardiol 2023; 20: 778-788.

[4] Litwin SE, Adams TD, Davidson LE, McKinlay R, Simper SC, Ranson L and Hunt SC. Longitudinal changes in cardiac structure and function in severe obesity: 11-year follow-up in the utah obesity study. J Am Heart Assoc 2020; 9: e014542.

[5] Walpot J, Inacio JR, Massalha S, El Mais H, Hossain A, Shiau J, Small GR, Crean AM, Yam Y, Rybicki F and Chow BJW. Early LV remodelling patterns in overweight and obesity: feasibility of cardiac CT to detect early geometric left ventricular changes. Obes Res Clin Pract 2019; 13: 478-485.

[6] Niedziela J, Hudzik B, Niedziela N, Gasior M, Gierlotka M, Wasilewski J, Myrda K, Lekston A, Polonski L and Rozentryt P. The obesity paradox in acute coronary syndrome: a meta-analysis. Eur J Epidemiol 2014; 29: 801-812.

[7] Galderisi M, Cosyns B, Edvardsen T, Cardim N, Delgado V, Di Salvo G, Donal E, Sade LE, Ernande L, Garbi M, Grapsa J, Hagendorff A, Kamp O, Magne J, Santoro C, Stefanidis A, Lancellotti P, Popescu B and Habib G; 2016-2018 EACVI Scientific Documents Committee; 2016-2018 EACVI Scientific Documents Committee. Standardization of adult transthoracic echocardiography reporting in agreement with recent chamber quantification, diastolic function, and heart valve disease recommendations: an expert consensus document of the European association of cardiovascular imaging. Eur Heart J Cardiovasc Imaging 2017; 18: 1301-1310.

[8] von Jeinsen B, Vasan RS, McManus DD, Mitchell GF, Cheng S and Xanthakis V. Joint influences of obesity, diabetes, and hypertension on indices of ventricular remodeling: findings from the community-based Framingham heart study. PLoS One 2020; 15: e0243199.

[9] Russo C, Jin Z, Homma S, Rundek T, Elkind MS, Sacco RL and Di Tullio MR. Effect of obesity and overweight on left ventricular diastolic function: a community-based study in an elderly cohort. J Am Coll Cardiol 2011; 57: 1368-1374.

[10] Freedman JE, Gerstein M, Mick E, Rozowsky J, Levy D, Kitchen R, Das S, Shah R, Danielson K, Beaulieu L, Navarro FC, Wang Y, Galeev TR, Holman A, Kwong RY, Murthy V, Tanriverdi SE, Koupenova-Zamor M, Mikhalev E and Tanriverdi K. Diverse human extracellular RNAs are widely detected in human plasma. Nat Commun 2016; 7: 11106.

[11] Schwarzenbach H, Nishida N, Calin GA and Pantel K. Clinical relevance of circulating cell-free microRNAs in cancer. Nat Rev Clin Oncol 2014; 11: 145-156.

[12] Trionfini P, Benigni A and Remuzzi G. MicroRNAs in kidney physiology and disease. Nat Rev Nephrol 2015; 11: 23-33.

[13] Waring ME, McManus RH, Saczynski JS, Anatchkova MD, McManus DD, Devereaux RS, Goldberg RJ, Allison JJ and Kiefe CI; TRACE-CORE Investigators. Transitions, risks, and actions in coronary events-center for outcomes research and education (TRACE-CORE): design and rationale. Circ Cardiovasc Qual Outcomes 2012; 5: e44-50.

[14] McManus DD, Saczynski JS, Lessard D, Waring ME, Allison J, Parish DC, Goldberg RJ, Ash A and Kiefe CI; TRACE-CORE Investigators. Reliability of predicting early hospital readmission after discharge for an acute coronary syndrome using claims-based data. Am J Cardiol 2016; 117: 501-507.

[15] McManus DD, Lin H, Tanriverdi K, Quercio M, Yin X, Larson MG, Ellinor PT, Levy D, Freedman JE and Benjamin EJ. Relations between circulating microRNAs and atrial fibrillation: data from the Framingham Offspring Study. Heart Rhythm 2014; 11: 663-669.

[16] Centers for Disease Control and Prevention. (2025). "BMI Categories". from https://www.cdc.gov/bmi/adult-calculator/bmi-categories.html.

[17] Lang RM, Badano LP, Mor-Avi V, Afilalo J, Armstrong A, Ernande L, Flachskampf FA, Foster E, Goldstein SA, Kuznetsova T, Lancellotti P, Muraru D, Picard MH, Rietzschel ER, Rudski L, Spencer KT, Tsang W and Voigt JU. Recommendations for cardiac chamber quantification by echocardiography in adults: an update from the American society of echocardiography and the European association of cardiovascular imaging. J Am Soc Echocardiogr 2015; 28: 1-39, e14.

[18] Devereux RB, Alonso DR, Lutas EM, Gottlieb GJ, Campo E, Sachs I and Reichek N. Echocardiographic assessment of left ventricular hypertrophy: comparison to necropsy findings. Am J Cardiol 1986; 57: 450-458.

[19] Wong N and Wang X. miRDB: an online resource for microRNA target prediction and functional annotations. Nucleic Acids Res 2015; 43: D146-152.

[20] Mi H and Thomas P. PANTHER pathway: an ontology-based pathway database coupled with data analysis tools. Methods Mol Biol 2009; 563: 123-140.

[21] Kramer A, Green J, Pollard J Jr and Tugendreich S. Causal analysis approaches in ingenuity pathway analysis. Bioinformatics 2014; 30: 523-530.

[22] Bartel DP. Metazoan MicroRNAs. Cell 2018; 173: 20-51.

[23] McMahon S, Charbonneau M, Grandmont S, Richard DE and Dubois CM. Transforming growth factor beta1 induces hypoxia-inducible factor-1 stabilization through selective inhibition of PHD2 expression. J Biol Chem 2006; 281: 24171-24181.

[24] Lee P, Chandel NS and Simon MC. Cellular adaptation to hypoxia through hypoxia inducible

factors and beyond. Nat Rev Mol Cell Biol 2020; 21: 268-283.
[25] Ho JJ, Metcalf JL, Yan MS, Turgeon PJ, Wang JJ, Chalsev M, Petruzziello-Pellegrini TN, Tsui AK, He JZ, Dhamko H, Man HS, Robb GB, Teh BT, Ohh M and Marsden PA. Functional importance of Dicer protein in the adaptive cellular response to hypoxia. J Biol Chem 2012; 287: 29003-29020.
[26] Garcia-Lacarte M, Mansego ML, Zulet MA, Martinez JA and Milagro FI. miR-1185-1 and miR-548q are biomarkers of response to weight loss and regulate the expression of GSK3B. Cells 2019; 8: 1548.
[27] Joshi A, Azuma R, Akumuo R, Goetzl L and Pinney SE. Gestational diabetes and maternal obesity are associated with sex-specific changes in miRNA and target gene expression in the fetus. Int J Obes (Lond) 2020; 44: 1497-1507.
[28] Zu Y, Wang Q and Wang H. Identification of miR-885-5p as a tumor biomarker: regulation of cellular function in cervical cancer. Gynecol Obstet Invest 2021; 86: 525-532.
[29] Zhang Z, Yin J, Yang J, Shen W, Zhang C, Mou W, Luo J, Yan H, Sun P, Luo Y, Tian Y and Xiang R. miR-885-5p suppresses hepatocellular carcinoma metastasis and inhibits Wnt/beta-catenin signaling pathway. Oncotarget 2016; 7: 75038-75051.
[30] Afanasyeva EA, Mestdagh P, Kumps C, Vandesompele J, Ehemann V, Theissen J, Fischer M, Zapatka M, Brors B, Savelyeva L, Sagulenko V, Speleman F, Schwab M and Westermann F. MicroRNA miR-885-5p targets CDK2 and MCM5, activates p53 and inhibits proliferation and survival. Cell Death Differ 2011; 18: 974-984.
[31] Ho JY, Hsu RJ, Wu CH, Liao GS, Gao HW, Wang TH and Yu CP. Reduced miR-550a-3p leads to breast cancer initiation, growth, and metastasis by increasing levels of ERK1 and 2. Oncotarget 2016; 7: 53853-53868.
[32] Guo ZZ, Ma ZJ, He YZ, Jiang W, Xia Y, Pan CF, Wei K, Shi YJ, Chen L and Chen YJ. miR-550a-5p functions as a tumor promoter by targeting LIMD1 in lung adenocarcinoma. Front Oncol 2020; 10: 570733.
[33] Tian Q, Liang L, Ding J, Zha R, Shi H, Wang Q, Huang S, Guo W, Ge C, Chen T, Li J and He X. MicroRNA-550a acts as a pro-metastatic gene and directly targets cytoplasmic polyadenylation element-binding protein 4 in hepatocellular carcinoma. PLoS One 2012; 7: e48958.
[34] Prastaro M, D'Amore C, Paolillo S, Losi M, Marciano C, Perrino C, Ruggiero D, Gargiulo P, Savarese G, Trimarco B and Perrone Filardi P. Prognostic role of transthoracic echocardiography in patients affected by heart failure and reduced ejection fraction. Heart Fail Rev 2015; 20: 305-316.
[35] Gaasch WH and Zile MR. Left ventricular structural remodeling in health and disease: with special emphasis on volume, mass, and geometry. J Am Coll Cardiol 2011; 58: 1733-1740.
[36] Verma A, Meris A, Skali H, Ghali JK, Arnold JM, Bourgoun M, Velazquez EJ, McMurray JJ, Kober L, Pfeffer MA, Califf RM and Solomon SD. Prognostic implications of left ventricular mass and geometry following myocardial infarction: the VALIANT (VALsartan In Acute myocardial iNfarcTion) Echocardiographic Study. JACC Cardiovasc Imaging 2008; 1: 582-591.
[37] Cohn JN, Ferrari R and Sharpe N. Cardiac remodeling--concepts and clinical implications: a consensus paper from an international forum on cardiac remodeling. Behalf of an International Forum on Cardiac Remodeling. J Am Coll Cardiol 2000; 35: 569-582.
[38] Parikh M and Pierce GN. A brief review on the biology and effects of cellular and circulating microRNAs on cardiac remodeling after infarction. Int J Mol Sci 2021; 22: 4995.
[39] Border WA and Noble NA. Transforming growth factor beta in tissue fibrosis. N Engl J Med 1994; 331: 1286-1292.
[40] Khalil H, Kanisicak O, Prasad V, Correll RN, Fu X, Schips T, Vagnozzi RJ, Liu R, Huynh T, Lee SJ, Karch J and Molkentin JD. Fibroblast-specific TGF-beta-Smad2/3 signaling underlies cardiac fibrosis. J Clin Invest 2017; 127: 3770-3783.
[41] Lyu G, Guan Y, Zhang C, Zong L, Sun L, Huang X, Huang L, Zhang L, Tian XL, Zhou Z and Tao W. TGF-beta signaling alters H4K20me3 status via miR-29 and contributes to cellular senescence and cardiac aging. Nat Commun 2018; 9: 2560.
[42] Zeisberg EM, Tarnavski O, Zeisberg M, Dorfman AL, McMullen JR, Gustafsson E, Chandraker A, Yuan X, Pu WT, Roberts AB, Neilson EG, Sayegh MH, Izumo S and Kalluri R. Endothelial-to-mesenchymal transition contributes to cardiac fibrosis. Nat Med 2007; 13: 952-961.
[43] John S, Bhowmick K, Park A, Huang H, Yang X and Mishra L. Recent advances in targeting obesity, with a focus on TGF-beta signaling and vagus nerve innervation. Bioelectron Med 2025; 11: 10.
[44] Yadav H, Quijano C, Kamaraju AK, Gavrilova O, Malek R, Chen W, Zerfas P, Zhigang D, Wright EC, Stuelten C, Sun P, Lonning S, Skarulis M, Sumner AE, Finkel T and Rane SG. Protection from obesity and diabetes by blockade of TGF-beta/Smad3 signaling. Cell Metab 2011; 14: 67-79.
[45] Lin Q, Huang Y, Booth CJ, Haase VH, Johnson RS, Celeste Simon M, Giordano FJ and Yun Z. Activation of hypoxia-inducible factor-2 in adi-

pocytes results in pathological cardiac hypertrophy. J Am Heart Assoc 2013; 2: e000548.
[46] Krishnan J, Suter M, Windak R, Krebs T, Felley A, Montessuit C, Tokarska-Schlattner M, Aasum E, Bogdanova A, Perriard E, Perriard JC, Larsen T, Pedrazzini T and Krek W. Activation of a HIF1alpha-PPARgamma axis underlies the integration of glycolytic and lipid anabolic pathways in pathologic cardiac hypertrophy. Cell Metab 2009; 9: 512-524.
[47] Montaigne D, Butruille L and Staels B. PPAR control of metabolism and cardiovascular functions. Nat Rev Cardiol 2021; 18: 809-823.
[48] Warbrick I and Rabkin SW. Hypoxia-inducible factor 1-alpha (HIF-1alpha) as a factor mediating the relationship between obesity and heart failure with preserved ejection fraction. Obes Rev 2019; 20: 701-712.
[49] Bergmann MW. WNT signaling in adult cardiac hypertrophy and remodeling: lessons learned from cardiac development. Circ Res 2010; 107: 1198-1208.
[50] Yousefi F, Shabaninejad Z, Vakili S, Derakhshan M, Movahedpour A, Dabiri H, Ghasemi Y, Mahjoubin-Tehran M, Nikoozadeh A, Savardashtaki A, Mirzaei H and Hamblin MR. TGF-beta and WNT signaling pathways in cardiac fibrosis: non-coding RNAs come into focus. Cell Commun Signal 2020; 18: 87.
[51] Qiu Y, Gan M, Wang X, Liao T, Chen Q, Lei Y, Chen L, Wang J, Zhao Y, Niu L, Wang Y, Zhang S, Zhu L and Shen L. The global perspective on peroxisome proliferator-activated receptor gamma (PPARgamma) in ectopic fat deposition: a review. Int J Biol Macromol 2023; 253: 127042.
[52] Bhandary B, Meng Q, James J, Osinska H, Gulick J, Valiente-Alandi I, Sargent MA, Bhuiyan MS, Blaxall BC, Molkentin JD and Robbins J. Cardiac fibrosis in proteotoxic cardiac disease is dependent upon myofibroblast TGF -beta signaling. J Am Heart Assoc 2018; 7: e010013.
[53] Prabhu SD and Frangogiannis NG. The biological basis for cardiac repair after myocardial infarction: from inflammation to fibrosis. Circ Res 2016; 119: 91-112.
[54] Abozaid YJ, Zhang X, Mens MMJ, Ahmadizar F, Limpens M, Ikram MA, Rivadeneira F, Voortman T, Kavousi M and Ghanbari M. Plasma circulating microRNAs associated with obesity, body fat distribution, and fat mass: the Rotterdam Study. Int J Obes (Lond) 2022; 46: 2137-2144.
[55] Mick E, Shah R, Tanriverdi K, Murthy V, Gerstein M, Rozowsky J, Kitchen R, Larson MG, Levy D and Freedman JE. Stroke and circulating extracellular RNAs. Stroke 2017; 48: 828-834.

Supplementary Table 2. miR and echo parameter hits

MiRNA	Number of Echo parameter hits
hsa_miR_10a_5p	2
hsa_miR_10b_5p	1
hsa_miR_1246	1
hsa_miR_1247_5p	1
hsa_miR_1271_5p	1
hsa_miR_142_5p	1
hsa_miR_144_5p	1
hsa_miR_148b_3p	1
hsa_miR_152_3p	1
hsa_miR_17_3p	1
hsa_miR_185_3p	2
hsa_miR_186_5p	1
hsa_miR_190a_3p	4
hsa_miR_200b_3p	1
hsa_miR_210_3p	2
hsa_miR_2110	2
hsa_miR_212_3p	1
hsa_miR_224_5p	2
hsa_miR_29b_3p	2
hsa_miR_29c_3p	2
hsa_miR_29c_5p	2
hsa_miR_320d	1
hsa_miR_337_3p	2
hsa_miR_342_5p	1
hsa_miR_34a_3p	2
hsa_miR_424_3p	1
hsa_miR_425_5p	1
hsa_miR_4446_3p	1
hsa_miR_450b_5p	1
hsa_miR_454_3p	2
hsa_miR_4770	1
hsa_miR_494_3p	2
hsa_miR_497_5p	1
hsa_miR_532_5p	1
hsa_miR_545_5p	1
hsa_miR_548d_3p	1
hsa_miR_584_5p	1
hsa_miR_590_3p	1
hsa_miR_596	3
hsa_miR_642a_5p	2
hsa_miR_656_3p	1
hsa_miR_6803_3p	1
hsa_miR_877_3p	1
hsa_miR_885_5p	4
hsa_miR_9_3p	1

Bolded are miRs with ≥3 echo parameter hits

Supplementary Table 3. Toxicity pathways and involved molecules

Ingenuity Toxicity Pathway	-log (*p*-value)	Ratio	Molecules
Renal Necrosis/Cell Death	9.49	0.132	AAK1,AGER,ATXN3,BCL6,BNIP3L,CALCR,CDKN1B,CDON,CEBPB,CEBPD,CTNNB1,CYBB,DDX21,E2F6,ERBB4,ETV5,EZR,FAT1,FLT1,FOXO1,FOXO3,FTO,GLS,GNAQ,GRM1,GSK3B,HIP1,HNF1B,HNRNPU,HSP90B1,IAPP,IRF4,IRS1,ITGB1,KMT2A,LRP6,LRRK2,MAGT1,MAP2K4,MAP3K1,MAP3K5,MAPK8,MCU,MIB1,MTOR,NRG1,NTRK2,NUP98,PAK2,PARVA,PDCD6IP,PPM1A,PPP3R1,PRKCA,PRKCD,PSIP1,PTCH1,PTGIS,PTPN6,RAD21,RBM7,RET,RGS4,RNF216,ROCK2,SALL1,SAP30L,SELENOT,SLC22A3,SLC25A11,SLC8A1,SMAD7,SRF,STAU1,TAF4B,TCF3,TCF4,TET1,TFRC,TIAM1,TLR4,TMEFF2,TMEM123,TP53INP1,USP14,USP38,VPS13A,WT1,WTAP,XIAP,YY1,ZBTB33,ZC3HAV1
RAR Activation	6.91	0.133	ACVR1,ADCY7,AKT3,ARID1A,ARID2,BMPR2,CDKN1B,CREB5,CREBBP,DKK2,ERCC3,GNAQ,GPCPD1,GTF2H3,GUCY1A1,GUCY1B1,HNF1B,HOXA4,HOXA5,IL33,KAT2B,KIT,MAP2K4,MAP3K1,MAP3K5,MAPK1,MAPK13,MAPK8,MEIS1,MMP11,NR2C1,NR2F2,NRIP1,PAX6,PBRM1,PDE10A,PDE11A,PDE1A,PDE2A,PDE5A,PDE7A,PDE7B,PIK3C2A,PIK3R4,PITX2,PNRC1,PRDM16,PRKACB,PRKCA,PRKCD,PRKCI,RAB11FIP3,REL,RET,RHOBTB1,RHOQ,RORB,SMARCA4,SMARCD2,SMARCE1,SOX9,TGFB3,TGFBR1,TGFBR3
Cardiac Hypertrophy	5.71	0.132	BMPR2,CACNA2D1,CACNB2,CASQ2,CDK13,DACT1,DICER1,ECE1,EGLN1,F2R,FBXO32,FNIP1,FOXO1,FOXO3,GNAQ,GSK3B,GUCY1A1,HDAC9,HEXIM1,HMGB1,HMGCR,HTR2C,IL1RL1,IL33,IL6R,IL6ST,MAP2K4,MAP3K5,MAPK1,MAPK8,MBNL1,MBNL2,MEF2C,MTOR,NCF1,NFATC2,NR3C2,PDE5A,PLN,PRKCA,PRKG1,RAB11FIP3,RAB2A,RGS4,ROCK2,SLC8A1,SMAD7,SMARCA4,SP3,TGFBR3,TIAM1,TLR4,VIP
Increases Glomerular Injury	5.65	0.162	ABL1,ADM,AGER,CD24,CDKN1B,CEBPB,CMIP,COL4A3,CTNNB1,ETV5,FLT1,FTO,GP1BA,HDAC9,IRAK3,IRF5,ITGB1,KMT2A,LYPLA1,MTOR,NR2F2,PFKFB3,PRKCD,PTPN6,PTPRB,SDK1,SMAD7,TCF4,TFRC,UBXN7,VNN1,WNT5A,WWTR1
Liver Proliferation	4.79	0.136	AHR,BMP7,CDKN1B,CEBPB,CIT,CNR1,CTNNB1,DICER1,DLC1,ENTPD5,ERO1A,FBXO45,FGF18,FGF7,FGFR2,FLT1,GSK3B,HMGB1,HMGCR,IL6R,IL6ST,IQGAP2,ITGA6,ITGB1,KITLG,MAP2K4,MAPK1,MAPK8,MET,NCF1,NTS,PROX1,PTPN6,RB1CC1,RTN4,SMAD7,SPTBN1,TOB1,WTAP,XDH
Cardiac Fibrosis	4.6	0.126	ABHD5,AGER,AHR,AKTIP,BCL6,BMPR1A,C1QBP,CDON,CYBB,DAG1,DICER1,DTNA,ELAVL1,FGFR1,FLT1,GSK3B,HEXIM1,ITGB1,MAP3K5,MAPK8,MBNL1,MBNL2,MEF2D,NCF1,NR3C2,OTUD1,PLN,PPM1L,PPP1CB,PRDM16,PRKG1,RANGRF,RBPJ,SAV1,SGCD,SGCG,SLC8A1,SMAD7,SMARCA4,TEAD1,THBS2,TIMP3,TLR4,TMEM65,TRPA1,UTRN,VGLL3
Increases Cardiac Proliferation	4.56	0.192	BMPR1A,CCBE1,CTNNB1,DICER1,ERBB4,FGFR1,FGFR2,GNAQ,GNL3,HOXA4,MAPK1,MEF2C,MYCN,NRG1,PRKCA,PROX1,RBPJ,TGFBR3,WNT2
TGF-β Signaling	4.49	0.19	ACVR1,BMP7,BMPR1A,BMPR2,CREBBP,MAP2K4,MAPK1,MAPK13,MAPK8,PITX2,RAP1A,RAP1B,RNF111,RRAS,SMAD5,SMAD7,TGFB3,TGFBR1,TRAF6
Cardiac Necrosis/Cell Death	3.84	0.12	ABCB8,ADM,BNIP3L,CACNB2,CALCRL,CCNT1,CDKN1B,CTNNB1,CXADR,CYBB,DICER1,EGLN1,ELAVL1,FBXO32,FOXO1,FOXO3,GNAQ,GSK3B,IL33,IL6ST,IQGAP1,LAMP2,LRP1,MAP2K4,MAP3K1,MAP3K5,MAPK1,MAPK8,MEF2D,MYH10,NRG1,PHB1,PRKCD,PROX1,RTN4,SGCD,SLC8A1,SMARCA4,THBD,THBS2,TLR4,XDH,XIAP
Increases Cardiac Dysfunction	3.34	0.161	CACNB2,CCR2,CYBB,DUSP6,ELAVL1,F2R,FOXO1,GNAQ,GSK3B,HTR4,MAP3K5,MEIS1,NCF1,NR3C2,PDE5A,PLN,ROCK2,TLR4
Hepatic Fibrosis	3.23	0.108	AHR,ASIC1,CCL7,CD24,CD38,CNR1,COL4A1,COL4A3,CTLA4,CTNNB1,DENND1B,ECE1,F2R,FBN1,FCRL3,FGF7,FGFR1,FRZB,GBP2,HMGCR,HSD17B13,IL33,IQCJ-SCHIP1,IRF5,ITGA6,JAG2,KLF3,MTTP,NDFIP1,NR3C1,PAH,PDE7B,PPP3R1,PTCH1,PTGER3,REL,RET,RPGRIP1L,SLC6A2,SMAD7,SRSF2,ST8SIA4,TAF4B,TGFB3,THBS2,TIMP3,TLR4,UBE2K,WNT2,WNT5A
Cell Cycle: G1/S Checkpoint Regulation	3.23	0.188	ABL1,CDKN1B,E2F5,E2F6,E2F8,FOXO1,GNL3,GSK3B,HDAC9,NRG1,RBL1,RBL2,TGFB3
p53 Signaling	3.06	0.162	AKT3,CSNK1D,CTNNB1,DRAM1,GNL3,GSK3B,HDAC9,JMY,KAT2B,MAPK8,MDM4,PIK3C2A,PIK3R4,TOPBP1,TP53INP1,WT1
Liver Necrosis/Cell Death	2.97	0.11	ABL1,ADAMTS3,ADM,AGER,AHR,CCR2,CDKN1B,CEBPB,CIT,CTNNB1,DICER1,EIF2AK3,ENTPD5,FGL2,FOXO3,GSK3B,HMGB1,HNRNPU,IL33,IL6R,IL6ST,IQGAP2,IRF5,LAMP2,LRP1,MAML1,MAP2K4,MAP3K5,MAPK8,MET,MTOR,MYCN,NCF1,NR2C1,RB1CC1,REL,SOX9,SPTBN1,TIMP3,TLR4,VASN,XIAP
PPARα/RXRα Activation	2.77	0.126	ACVR1,ADCY7,BMPR2,CREBBP,GNAQ,GUCY1A1,GUCY1B1,HSP90B1,IL1RL1,IRS1,MAP2K4,MAPK1,MAPK8,MED23,MEF2C,PRKACB,PRKCA,RAP1A,RAP1B,REL,RRAS,TGFB3,TGFBR1,TGFBR3,TRAF6
VDR/RXR Activation	2.71	0.167	CDKN1B,CEBPB,FOXO1,HOXA10,IL1RL1,MXD1,PRKCA,PRKCD,PRKCI,PRKD3,THBD,WT1,YY1
Hypoxia-Inducible Factor Signaling	2.65	0.171	ASPH,CSNK1D,EIF1AX,EIF2S1,ELAVL1,FLT1,HIF1AN,PRKCA,UBE2B,UBE2D1,UBE2H,UBE2N

Increases Liver Steatosis	2.57	0.128	AHR,CCR2,CD38,CNR1,ELOVL2,FERMT2,FOXO1,HSD17B13,IL6ST,IRF4,MAP3K5,MAPK13,MAPK8,ME1,MED13,NR3C1,NRIP1,RBM38,RBPJ,RICTOR,SPTBN1,USP14
Hepatic Cholestasis	2.32	0.116	ADCY7,AKT3,CFTR,CHP1,FOXO1,GUCY1A1,GUCY1B1,IL1RL1,IL33,IL6R,IRAK3,MAP2K4,MAPK1,MAPK8,NR5A2,PPP3R1,PRKACB,PRKCA,PRKCD,PRKCI,PRKD3,REL,TGFB3,TLR4,TNFRSF11B,TRAF6
Long-term Renal Injury Pro-oxidative Response Panel (Rat)	2.05	0.308	CYBB,FMO5,NCF1,XDH
Increases Liver Hyperplasia/Hyperproliferation	2.03	0.112	AHR,CCR2,CDKN1B,CTNNB1,FBXO45,HMGB1,HMGCR,HNRNPA1,HNRNPA2B1,IL6ST,IQGAP1,MAPK1,MAPK8,MEF2D,MET,MSI2,MTOR,NR5A2,SPTBN1,TEAD1,TLR4,TRIM33,VCAN,YTHDF3
Renal Glomerulus Panel (Human)	1.63	0.235	DAG1,PDPN,PTPRO,WT1
NRF2-mediated Oxidative Stress Response	1.57	0.0993	CCT7,CREBBP,DNAJA2,DNAJB12,DNAJB14,DNAJB4,DNAJC15,EIF2AK3,ENC1,GSK3B,HSP90B1,MAP2K4,MAP3K1,MAP3K5,MAPK1,MAPK8,PIK3C2A,PIK3R4,PRKCA,PRKCD,PRKCI,PRKD3,RAP1A,RAP1B,RRAS,UBE2K,USP14
Increases Heart Failure	1.57	0.192	CACNB2,DUSP6,E2F6,PLN,PRKCA
Decreases Transmembrane Potential of Mitochondria and Mitochondrial Membrane	1.37	0.106	BNIP3L,CCNT1,CD47,FOXO1,IL7,IRF5,IRS1,MAP2K4,MAPK13,MAPK8,MYCN,PDK1,PRKCD,RTN4,TCF3,TIMP3,XDH
Increases Renal Proliferation	1.22	0.0984	ARHGEF7,CAMK4,CD24,CEBPB,CTNNB1,DDX21,HAS2,IGF2BP3,ITGB1,MTOR,NUP98,ROCK2,SDCBP,STAU1,TFAP2A,TLR4,TMEFF2,TRPA1,USP7
Cell Cycle: G2/M DNA Damage Checkpoint Regulation	1.2	0.132	ABL1,KAT2B,MDM4,MYT1,YWHAB,YWHAE,YWHAH
Hepatic Stellate Cell Activation	1.09	0.143	LHX2,TGFB3,TGFBR1,TGFBR3,TLR4
Xenobiotic Metabolism Signaling	0.916	0.0829	AHR,ALDH1L2,ANKRA2,CAMK4,CREBBP,CYP19A1,EIF2AK3,FMO5,GRIP1,HS3ST3B1,HS3ST4,HSP90B1,MAP2K4,MAP3K1,MAP3K5,MAPK1,MAPK13,MAPK8,NRIP1,PIK3C2A,PIK3R4,PPM1L,PPP2CB,PPP2R2A,PPP2R5E,PRKCA,PRKCD,PRKCI,PRKD3,RAP1A,RAP1B,REL,RRAS
Increases Renal Damage	0.823	0.0938	ABL1,ADM,CCR2,CTNNB1,ITGB1,LRRK2,NR3C2,POU2F1,PTPRB,SLC8A1,TLR4,WTAP
Genes associated with Chronic Allograft Nephropathy (Human)	0.788	0.143	CCR2,COL4A1,VCAM1
Anti-Apoptosis	0.785	0.125	BAG2,BFAR,TNFAIP8,XIAP
Increases Cardiac Dilation	0.742	0.105	F2R,GNAQ,MAP3K5,NCF1,PRKCA,SAV1
Increases Transmembrane Potential of Mitochondria and Mitochondrial Membrane	0.616	0.1	ABL1,ARID1A,PHB1,PTPN6,YWHAE
Renal Proximal Tubule Toxicity Biomarker Panel (Rat)	0.569	0.111	SLC16A7,SLC25A11,SLC34A2
Mechanism of Gene Regulation by Peroxisome Proliferators via PPARα	0.516	0.0842	CREBBP,FAT1,MAPK1,ME1,NRIP1,PRKACB,PRKCA,TRAF6
Pro-Apoptosis	0.509	0.0952	BNIP3L,DEDD,ERCC3,FOXO3
Cytochrome P450 Panel - Substrate is an Eicosanoid (Mouse)	0.468	0.167	PTGIS
Cytochrome P450 Panel - Substrate is a Vitamin (Human)	0.468	0.167	CYP26B1
Aryl Hydrocarbon Receptor Signaling	0.455	0.0761	AHR,ALDH1L2,CDKN1B,DHFR,HSP90B1,HSPB7,MAPK1,MAPK8,NRIP1,RBL1,RBL2,REL,SMARCA4,TGFB3
Increases Renal Nephritis	0.424	0.0811	CD24,COL4A3,FTO,GP1BA,IRF5,TCF4
TR/RXR Activation	0.417	0.0763	AKT3,CAMK4,MBP,ME1,MTOR,PCK1,PIK3C2A,PIK3R4,TBL1XR1,THRB
Cytochrome P450 Panel - Substrate is an Eicosanoid (Human)	0.415	0.143	PTGIS
Cytochrome P450 Panel - Substrate is a Vitamin (Mouse)	0.415	0.143	CYP26B1
Cytochrome P450 Panel - Substrate is a Vitamin (Rat)	0.415	0.143	CYP26B1
Increases Bradycardia	0.407	0.1	CYBB,HTR2A
Biogenesis of Mitochondria	0.407	0.1	CAV2,CXADR

Acute Renal Failure Panel (Rat)	0.395	0.0806	ADM,ANXA1,LIFR,SLC16A7,VCAM1
Vasopressin-induced Genes in Inner Medullary Renal Collecting Duct Cells (Rat)	0.371	0.125	PRKACB
Increases Liver Damage	0.32	0.0714	HMGB1,IL6ST,MAPK8,MET,NCF1,SORT1,SOX9,TLR4
PXR/RXR Activation	0.316	0.0735	AKT3,FOXO1,FOXO3,NR3C1,PRKACB
Cytochrome P450 Panel - Substrate is a Fatty Acid (Human)	0.301	0.1	PTGIS
Renal Ischemic Resistance Panel (Rat)	0.301	0.1	FBN1
Increases Liver Hepatitis	0.285	0.0687	CBLB,CNR1,HMGB1,MAPK8,MTTP,NUP98,TFRC,TLR4,XIAP
Primary Glomerulonephritis Biomarker Panel (Human)	0.273	0.0909	SAMD4A
Cytochrome P450 Panel - Substrate is a Sterol (Human)	0.207	0.0714	CYP19A1
Cytochrome P450 Panel - Substrate is a Sterol (Mouse)	0.207	0.0714	CYP19A1
Cytochrome P450 Panel - Substrate is a Sterol (Rat)	0.207	0.0714	CYP19A1
Recovery from Ischemic Acute Renal Failure (Rat)	0.207	0.0714	COL4A1
LPS/IL-1 Mediated Inhibition of RXR Function	0	0.0459	ACSL3,ALDH1L2,FMO5,HS3ST3B1,HS3ST4,IL1RL1,IL33,MAP2K4,MAP3K1,MAPK8,NR5A2,TLR4,TNFRSF11B,TRAF6
NF-κB Signaling	0	0.047	AKT3,BMPR1A,BMPR2,CREBBP,FGFR1,FGFR2,FLT1,GSK3B,IL33,IRAK3,MAP3K1,MAPK6,MAPK8,NTRK2,PIK3C2A,PIK3R4,PRKACB,RAP1A,RAP1B,RRAS,TANK,TGFBR1,TGFBR3,TLR4,TNFRSF11B,TRAF6,UBE2N
Cholesterol Biosynthesis	0	0.0625	HMGCR
Fatty Acid Metabolism	0	0.0259	ACADSB,ACSL3,CYP19A1
Oxidative Stress	0	0.0526	ME1,VCAM1,XDH
CAR/RXR Activation	0	0.0345	PCK1
LXR/RXR Activation	0	0.0538	CCL7,HMGCR,IL1RL1,IL33,REL,TLR4,TNFRSF11B
FXR/RXR Activation	0	0.0612	AKT3,CREBBP,CYP19A1,EIF2AK3,FOXO1,HMGB1,IL33,MAP2K4,MAPK8,MTTP,NR5A2,TGFB3
Mitochondrial Dysfunction	0	0.0646	ATP12A,ATP1A2,BACE1,CACNA2D1,CACNB2,CHP1,COX5A,CREB5,CREBBP,DLD,LRRK2,MAP2K4,MAP3K5,MAPK8,MCU,MTOR,OPA1,PDHB,PIK3C2A,PIK3R4,PPP3R1,PRKACB,XDH
Decreases Respiration of Mitochondria	0	0.0556	MAPK8
Decreases Depolarization of Mitochondria and Mitochondrial Membrane	0	0.0513	PHB1,VPS13A
Nongenotoxic Hepatocarcinogenicity Biomarker Panel	0	0.0455	TRNT1
Persistent Renal Ischemia-Reperfusion Injury (Mouse)	0	0.0667	SOX9,VCAM1

Supplementary Table 4. PANTHER Analysis

PANTHER Biological Process	Raw *p* value	-log(p)
Alzheimer disease-presenilin pathway	3.83E-03	2.41680123
Interferon-gamma signaling pathway	3.62E-03	2.44129143
Interleukin signaling pathway	1.83E-03	2.73754891
Endothelin signaling pathway	1.72E-03	2.76447155
RAS pathway	1.55E-03	2.8096683
Alzheimer disease-amyloid secretase pathway	1.53E-04	3.81530857
Angiogenesis	9.42E-05	4.0259491
Gonadotropin-releasing hormone receptor pathway	9.00E-05	4.04575749
CCKR signaling map	6.30E-05	4.20065945
FGF signaling pathway	6.31E-06	5.19997064
EGF receptor signaling pathway	4.66E-06	5.33161408
WNT signaling pathway	6.44E-08	7.19111413